

To appear in ApJ Letters.

Detection of sub-TeV Gamma-rays from the Galactic Center Direction by CANGAROO-II

K. Tsuchiya¹, R. Enomoto¹, L.T. Ksenofontov¹, M. Mori¹, T. Naito², A. Asahara³,
G.V. Bicknell⁴, R.W. Clay⁵, Y. Doi⁶, P.G. Edwards⁷, S. Gunji⁶, S. Hara¹, T. Hara²,
T. Hattori⁸, Sei. Hayashi⁹, C. Itoh¹⁰, S. Kabuki¹, F. Kajino⁹, H. Katagiri¹, A. Kawachi¹,
T. Kifune¹¹, H. Kubo³, T. Kurihara⁸, R. Kurosaka¹, J. Kushida⁸, Y. Matsubara¹²,
Y. Miyashita⁸, Y. Mizumoto¹³, H. Moro⁸, H. Muraishi¹⁴, Y. Muraki¹², T. Nakase⁸,
D. Nishida³, K. Nishijima⁸, M. Ohishi¹, K. Okumura¹, J.R. Patterson⁵, R.J. Protheroe⁵,
N. Sakamoto⁶, K. Sakurazawa¹⁵, D.L. Swaby⁵, T. Tanimori³, H. Tanimura³, G. Thornton⁵,
F. Tokanai⁶, T. Uchida¹, S. Watanabe³, T. Yamaoka⁹, S. Yanagita¹⁶, T. Yoshida¹⁶,
T. Yoshikoshi¹⁷

¹ICRR, Univ. of Tokyo, Kashiwa, Chiba 277-8582, Japan; tsuchiya@icrr.u-tokyo.ac.jp, enomoto@icrr.u-tokyo.ac.jp

²Fac. of Management Information, Yamanashi Gakuin Univ., Yamanashi 400-8575, Japan

³Dept. of Phys., Grad. School of Sci., Kyoto Univ., Kyoto 606-8502, Japan

⁴RSAA, Australian National Univ., ACT 2611, Australia

⁵Dept. of Physics, Univ. of Adelaide, SA 5005, Australia

⁶Dept. of Phys., Yamagata Univ., Yamagata 990-8560, Japan

⁷ISAS/JAXA, Sagamihara, Kanagawa 229-8510, Japan

⁸Dept. of Phys., Tokai Univ., Kanagawa 259-1292, Japan

⁹Dept. of Phys., Konan Univ., Hyogo 658-8501, Japan

¹⁰Ibaraki Prefectural Univ. of Health Sci., Ibaraki 300-0394, Japan

¹¹Fac. of Engineering, Shinshu Univ., Nagano 480-8553, Japan

¹²STE Lab., Nagoya Univ., Aichi 464-8602, Japan

¹³NAOJ, Mitaka, Tokyo 181-8588, Japan

¹⁴School of Allied Health Sci., Kitasato Univ., Kanagawa 228-8555, Japan

¹⁵Dept. of Phys., TIT, Tokyo 152-8551, Japan

¹⁶Fac. of Sci., Ibaraki Univ., Ibaraki 310-8512, Japan

¹⁷Dept. of Phys., Osaka City Univ., Osaka 558-8585, Japan

ABSTRACT

We have detected sub-TeV gamma-ray emission from the direction of the Galactic Center (GC) using the CANGAROO-II Imaging Atmospheric Cherenkov Telescope (IACT). We detected a statistically significant excess at energies greater than 250 GeV. The flux was one order of magnitude lower than that of Crab at 1 TeV with a soft spectrum $\propto E^{-4.6 \pm 0.5}$. The signal centroid is consistent with the GC direction and the observed profile is consistent with a point-like source. Our data suggests that the GeV source 3EG J1746–2851 is identical with this TeV source and we study the combined spectra to determine the possible origin of the gamma-ray emission. We also obtain an upper limit on the cold dark-matter density in the Galactic halo.

Subject headings: gamma rays: observation — Galaxy: center

1. Introduction

Many observations have been made of the Galactic Center (GC) region over a wide range of wavelengths (e.g., Pauls et al. 1976; Sofue et al. 1986; Pedlar et al. 1989; Koyama et al. 1996; Buckley et al. 1997; Purcell et al. 1997; Mayer-Hasselwander et al. 1998; Maeda et al. 2002). At the dynamical center of the Galaxy is the source Sgr A*, containing a $4 \times 10^6 M_\odot$ black hole, which is a strong, variable, radio source (e.g., Zhao et al. 2003) and a weak, but occasionally flaring, infra-red (Genzel et al. 2003) and X-ray (Baganoff et al. 2001) source. Surrounding Sgr A* are the (presumed) supernova remnant Sgr A East, and a number of filamentary radio structures, including one known as the Arc, extending over tens of parsecs. One filamentary structure was recently found to be a non-thermal X-ray source (Sakano et al. 2003). The radio emission is interpreted as synchrotron radiation from high-energy electrons in the ambient magnetic fields. The observed magnetic fields are as high as several mG, although whether they are distributed over the whole GC region or are localized is not known (Morris 1994).

The bright EGRET source 3EG J1746–2851 is listed as unidentified in the third EGRET catalog (Hartman et al. 1999), but as the position, given in 3EG as ($l = 0.11, b = -0.04$) with an 95% confidence contour radius of 0.13 degrees, is consistent with the GC, it has been considered as the gamma-ray counterpart to GC region (Mayer-Hasselwander et al. 1998). Three different source scenarios were suggested by Mayer-Hasselwander et al. (1998): emission from one or more pulsars, inverse Compton radiation from relativistic electrons in the Arc, or Cold Dark Matter (CDM) annihilation. N-body simulations suggest a significant

enhancement of the CDM density around galaxy cores (Navarro, Frenk, & White 1996). Better constraints on CDM can be obtained by high-energy gamma-ray observations of the GC region. More recently, 3EG J1746–2851 has been associated with Sgr A East, with the gamma-ray emission arising from the decay of neutral pions produced by high-energy protons, accelerated in the remnant, interacting with the ambient matter (Fatuzzo & Melia 2003). Time variability was reported, although its amplitude is not large (Nolan et al. 2003).

Spectra derived from the EGRET data (Mayer-Hasselwander et al. 1998; Hartman et al. 1999, shown in Fig. 3) are not well fit by a single power-law: the spectra are quite hard at low energies but flatten, or possibly turn over, at high energies. Simple extrapolations of the high energy spectra, however, suggest a potentially detectable TeV flux.

We have observed the GC region with the CANGAROO-II Imaging Atmospheric Cherenkov Telescope (IACT). The 10 m diameter CANGAROO-II telescope (Kawachi et al. 2001) detects gamma-rays above several hundred GeV by detecting optical Cherenkov radiation generated by relativistic secondary particles in the cascades produced when high-energy gamma-rays (and background cosmic rays) interact with the Earth’s upper atmosphere. The optical images provide information on the direction and energy of gamma-ray events. The telescope is located near Woomera, South Australia ($136^{\circ}47' E$, $31^{\circ}06' S$) and thus the GC culminates within $\sim 2^{\circ}$ of the zenith, enabling observations with a lower energy threshold. Observations with the Whipple IACT from Mt Hopkins ($31^{\circ}58' N$) yielded an 2σ upper limit of $0.45 \times 10^{-11} \text{ cm}^{-2} \text{ s}^{-1}$ at 2 TeV (Buckley et al. 1997).

The angular resolution of CANGAROO-II is 0.24° (36 pc at a distance of 8.5 kpc) with an energy threshold of 400 GeV in the case of a Crab-like energy spectrum ($\propto E^{-2.5}$). For the softer spectrum, $\propto E^{-4.6}$, we find (see § 4), the angular resolution becomes 0.32° (47 pc at 8.5 kpc) and the energy threshold is lowered to 250 GeV. With this angular resolution we cannot resolve Sgr A* (~ 1 pc in size) and the elliptical Sgr A East (major axis of 10.5 pc), which surrounds Sgr A* (Yusef-Zadeh & Morris 1987; Maeda et al. 2002). The location of the EGRET source 3EG J1746–2851 is also too close to the GC for us to resolve it.

2. Observations

The observations were carried out during 2001 July 12–24 (13 nights), and between 2002 July 4 and August 11 (20 nights). The telescope tracked Sgr A* ($\alpha = 266.42^{\circ}$, $\delta = -29.01^{\circ}$, J2000 coordinates). The field of view (FOV) of the camera is $2.76^{\circ} \times 2.76^{\circ}$. The brightest star in the FOV (SAO 185755) has a visual magnitude of 4.7. Most stars in this region are reddened, and the camera is sensitive to UV light, however this region is brighter than our

typical on-source FOV. As a result, we used a higher trigger threshold, requiring 4 triggered pixels rather than the usual 3 (Itoh et al. 2003), which reduced the trigger rate from 17 to 6 Hz. Lights from the detention center located several kilometers from the telescope had little effect on these observations as the telescope was pointed close to the zenith (Itoh et al. 2003). This was checked from the azimuthal angle dependence of the shower rate (see § 3). Each night was divided into two or three periods, i.e., ON-OFF, OFF-ON-OFF, or OFF-ON observations. ON-source observations were timed to contain the meridian passage of the target, as was done by Enomoto et al. (2002b). In total, 7300 min. of ON- and 7100 min. of OFF-source data were obtained.

3. Analysis

First, ‘cleaning’ cuts on camera images were applied, requiring (0.115° -square) pixel pulse-heights of greater than 3.3 photoelectrons, and Cherenkov photon arrival times within ± 40 ns of the median arrival time. Clusters of at least five adjacent triggered pixels were required in each event (in contrast to our usual acceptance of clusters of at least four pixels) to minimize the effects of the bright star field. After these pre-selection cuts, the shower rate was stable on a run-to-run basis for observations in the same year. Events due to background light were reduced by 99.8% at this level. A difference of $18 \pm 14\%$ in the average shower rates for 2001 and 2002 was apparent at this stage. We interpret this as being due to a deterioration of the mirror reflectivity and/or camera sensitivity, of $-10.2 \pm 4.6\%$. This was taken into account in further analysis and included in the final systematic errors in Table 1. The systematic difference of the run-by-run acceptance within the same year is expected to be less than 8.4%. The ON/OFF shower rate difference was $(3 \pm 9)\%$. By examining the event rates within each run we were able to reject periods affected by cloud, dew forming on the mirrors, instrumental abnormalities, etc. Only data taken at elevation angles greater than 60° were accepted. After these cuts, 4000 min. of ON- and 3400 min. of OFF-source data survived.

Trigger rates for each pixel per $700\,\mu\text{s}$ were monitored by a scaler circuit in real-time and recorded each second. These data were used to exclude ‘hot’ pixels (generally due to the passage of a star through the FOV of a pixel) in off-line analysis. Hillas parameters were then calculated to discriminate gamma-rays from cosmic-rays based on the image shape and orientation (Hillas 1985). Further we masked a small number of pixels which showed deformed ADC spectra, possibly due to a hardware fault. Discrimination of the cosmic-ray background from gamma-rays was carried out using the likelihood method of Enomoto et al. (2002a).

Crab nebula data were analyzed with the same code, with the derived flux and morphology consistent with the previous measurements and the point-spread function, respectively. The distributions of the Hillas parameters for the excess events were checked and found to be consistent with Monte Carlo simulations for gamma rays. The OFF-source data were compared with the Monte Carlo simulations of protons, and found to be consistent.

4. Results

The resulting distributions of the image orientation angle, α , are shown in Fig. 1 for both years and for the combined data-set. The normalizations between the ON- and OFF-distributions were carried out using data with $\alpha > 30^\circ$. The numbers of excess events ($\alpha < 15^\circ$) were 800 ± 100 (in an observation time of 1400 min.), 860 ± 140 (2600 min.), and 1660 ± 170 (4000 min.) in 2001, 2002, and the combined data, respectively, where the quoted errors include only statistical ones. A difference in the excess rates for 2001 and 2002 is apparent, with the (2001/2002) ratio being 1.60 ± 0.34 . We note that a flare was observed at 1.3 mm from Sgr A* in July 2001 (Yuan & Zhao 2002). However the shower rate (effectively energy threshold) difference described above could affect this ratio at the 20% level. We are, thus, unable to infer that the TeV emission is from a variable source. Nightly signal rates were also checked during both years, even though these have poorer statistics. The largest deviation occurred on 2002 Aug 11, UT, with a rate 1.8 ± 0.6 times larger than the average for that year, again not statistically significant.

Our Monte Carlo simulations predict, for a point-source, that gamma-ray events with $\alpha < 15^\circ$ should constitute 73.5% of those with $\alpha < 30^\circ$. The experimental data yielded $80.8 \pm 6.7\%$, consistent with the point-source assumption. As a further check on the spatial distribution of the signal, we derived the “significance map”, as shown by the thick contours in Fig. 2. The contours were calculated from the distribution of the detection significance determined at each location from the difference in the α plots (ON- minus OFF-source histogram) divided by the statistical errors. The centroid is consistent with 3EG J1746–2851, within our possible systematic uncertainty of 0.1° , and so we identify the GeV source as the likely origin of the TeV emission. Our angular resolution was estimated to be 0.32° , slightly larger than the radius of the 65% contour, consistent with the point-source assumption. The acceptance of the CANGAROO-II telescope is a smoothly decreasing function with an offset from the tracking center, falling to 50% at a 0.9° offset (see Itoh et al. 2003, for details).

After correcting for this acceptance, the differential fluxes listed in Table 1 were derived. As both statistical and systematic errors are included, the energy bins overlap somewhat, particularly at low energies. The systematic uncertainty for the energy determination ($\sim 20\%$),

which is an overall factor, dominates the errors in the energies. The Spectral Energy Distribution (SED) is plotted in Fig. 3 together with the EGRET data (Mayer-Hasselwander et al. 1998; Hartman et al. 1999). The cross-hatched area indicates the CANGAROO-II data reported here. The derived spectrum has a power-law index of -4.6 ± 0.5 , much softer than that of the Crab nebula (-2.5). When considered together with the EGRET data it is clear the flux falls off steeply in the TeV region.

Various checks on the signal level and position were carried out, by varying thresholds, clustering cuts, Hillas parameter values, etc: these yielded consistent fluxes within the systematic errors given in Table 1.

5. Discussion

Due to the complex structure of the GC region different scenarios for the origin of the EGRET gamma-ray flux have been considered (see, e.g., Mayer-Hasselwander et al. 1998, and references therein). As mentioned in §1, Fatuzzo & Melia (2003) have recently attributed the GeV emission to π^0 decay resulting from high-energy protons interacting with the ambient matter in Sgr A East. They argued that due to synchrotron cooling in the high average magnetic field, primary (accelerated) and secondary leptons would have a steep spectrum, and their contribution to the high energy gamma-ray flux via inverse Compton emission and bremsstrahlung would be small. The leptonic contribution to the TeV gamma-ray flux would be even smaller. Indeed, the synchrotron cooling time can be estimated as $\tau_s = 16 \times B_{mG}^{-2} E_{e,TeV}^{-1}$ yr. Thus for leptons of a few TeV, which might contribute to the sub-TeV gamma-ray flux, the cooling time in a mG magnetic field is even less than those considered by Fatuzzo & Melia (2003). Another factor which will reduce the amount of secondary TeV leptons, the key products from pp interactions, is the presence of a cut-off in the accelerated proton spectrum at a few TeV, suggested by this observation (see below). In the case of Sgr A*, an even higher magnetic field is expected, which would lead to the same conclusion.

In Fig. 3 we reproduce the π^0 decay emission to fit both the EGRET data and ours. The input proton spectrum was assumed to be proportional to $E^{-\gamma} e^{-E/E_{max}}$. The number density of the ambient gas (n) was taken to be $\sim 10^3$ cm $^{-3}$ (Maeda et al. 2002), however this affects only the estimation of the total proton cosmic-ray energy, as $E_c \propto n^{-1}$. The various lines shown in Fig. 3 are for differing values of γ and E_{max} . The GeV spectrum given in the 3EG catalog (Hartman et al. 1999) differs from that of the dedicated analysis of Mayer-Hasselwander et al. (1998), however, in both cases the EGRET and CANGAROO-II data can be relatively smoothly connected, with a cutoff energy of 1–3 TeV. The spectra for

$\gamma = 2.4$ yield slightly worse fits to the data at the lowest energies. The inferred total cosmic-ray energy greater than 1 GeV (see Fig. 3) corresponds to $\leq 10\%$ of a typical supernova energy, a quite plausible conversion efficiency. The details, however, are dependent on the EGRET flux. In the case of a lower gas density (n), the cosmic ray energy exceeds that of a single supernova, and we should consider the possibility of other sources in the GC region, such as Sgr A* itself, contributing to the gamma-ray flux. Our data determine the maximum energy to which cosmic rays are accelerated in this region, which does not depend upon other physical parameters. For example, the range of values is consistent with recent theoretical predictions for shock acceleration in supernova remnants (Ptuskin & Zirakashvili 2003).

Thus, identifying the TeV source with 3EG J1746–2851, and associating these in turn with Sgr A East and/or Sgr A*, we find that the gamma-ray fluxes and spectra can be naturally explained as arising due to π^0 decay.

We can, in addition, use our observations to derive upper limits to the CDM abundance in the GC region, assuming the GeV and TeV emission is centered on Sgr A* and following the method of Enomoto et al. (2003). The emission region is assumed to be a sphere with a radius of 47 pc. The annihilation mode of $\chi\chi \rightarrow q\bar{q}$ was first considered. The cross section (σ) multiplied by the relative velocity (v) and the branching fraction (B) is a free parameter that was normalized to $10^{-26} \text{ cm}^3 \text{ s}^{-1}$. The experimental data of $e^+e^- \rightarrow q\bar{q} \rightarrow \gamma X$ was used for the gamma-ray multiplicity (Ackestaff et al. 1998). The derived 2σ upper limits for the CDM densities ($\rho_{CDM}^{47pc} \sqrt{\sigma v B / 10^{-26} \text{ cm}^3 \text{ s}^{-1}}$) are 9300, 7300, 5800, 5300, and 5800 GeV/cm^3 for an assumed WIMP mass of 0.7, 1, 2, 4, and 6 TeV, respectively. Here, although we took the EGRET flux as an upper limit, above 0.6 TeV it is the CANGAROO-II data that dominates these results. Navarro, Frenk, & White (1996) and subsequent analyses (Fukushige & Makino 2003; Moore et al. 1999; Ghigna et al. 2000; Jing & Suto 2000; Power et al. 2003) adopted a cusp structure, i.e., the density profile proportional to $r^{-\beta}(1+r/r_s)^{\beta-3}$, where r_s is a free parameter and α ranges from 1 to 1.5. In the case of $\beta=1.3$, the upper limits of local densities ($\rho_{CDM}^{\odot} \sqrt{\sigma v B / 10^{-26} \text{ cm}^3 \text{ s}^{-1}}$) are of the order of several GeV/cm^3 . Higher upper limits are obtained when the decay mode of $\chi\chi \rightarrow \gamma\gamma$ was assumed with $\sigma v B_{\gamma\gamma} = 10^{-29} \text{ cm}^3 \text{ s}^{-1}$.

This work was supported by a Grant-in-Aid for Scientific Research by the Japan Ministry of Education, Culture, Sports, Science and Technology, and by JSPS Research Fellowships. This work was also supported by ARC Linkage Infrastructure Grant LE0238884 and Discovery Project Grant DP0345983. We thank the Defense Support Center Woomera and BAE Systems.

REFERENCES

Ackerstaff, K., et al. 1998, *Eur. Phys. J. C5*, 411

Baganoff, F.K., et al. 2001, *Nature*, 413, 45

Buckley, J.H., et al. 1997, *Proc. 25th ICRC (Durban)*, 3, 237

Enomoto, R., Hara, S., et al. 2002a, *Astropart. Phys.*, 16, 235

Enomoto, R., et al. 2002b, *Nature*, 416, 823

Enomoto, R., Yoshida, T., Yanagita, S., & Itoh, C. 2003, *ApJ*, 596, 216

Fatuzzo, M., & Melia, F. 2003, *ApJ*, 596, 1035

Fukushige, T., & Makino, J. 2003, *ApJ*, 588, 674

Genzel, R., et al. 2003, *Nature*, 425, 934

Ghigna, S., et al. 2000, *ApJ*, 544, 616

Hartman, R.C., et al. 1999, *ApJS*, 123, 79

Hillas, A.M., *Proc. 19th ICRC (La Jolla)*, 3, 445

Itoh, C., et al., 2003, *A&A*, 402, 443

Jing, Y.P., & Suto, Y. 2000, *ApJ*, 529, L69

Kawachi, A., et al. 2001, *Astropart. Phys.*, 14, 261

Koyama, K., et al. 1996, *PASJ*, 48, 249

Maeda, Y., et al. 2002, *ApJ*, 570, 671

Mayer-Hasselwander, H.A., et al. 1998, *A&A*, 335, 161

Moore, B., et al. 1999, *MNRAS*, 310, 1147

Morris, M., 1994, *The Nuclei of Normal Galaxies*, eds R. Genzel & A.I. Harris, Kluwer, Dordrecht, 185

Navarro, J.F., Frenk, C.S., & White, S.D.M. 1996 *ApJ*, 462, 563

Nolan, P.L., Tompkins, W.F., Grenier I.A., & Michelson P.F. 2003 *ApJ*, 597, 615

Pauls, T., Downes, D., Mezger, P.G., & Churchwell, E. 1976, A&A, 46, 407

Pedlar, A., et al. 1989, ApJ, 342, 769

Power, C., et al. 2003, MNRAS, 338, 14

Ptuskin, B.S., & Zirakashvili, V.N. 2003, A&A, 403, 1

Purcell, W.R., et al. 1997, ApJ, 491, 725

Sakano, M., Warwick, R.S., Decourchelle, A., & Predehl, P. 2003, MNRAS, 340, 747

Schödel R. et al., 2002, Nature, 419, 694

Sofue, Y., et al. 1986, PASJ, 38, 475

Yuan, F., & Zhao, J.-H. 2002, astro-ph/0203050

Yusef-Zadeh, F. & Morris, M. 1987, ApJ, 320, 545

Zhao, J.-H., et al. 2003, ApJ, 586, L29

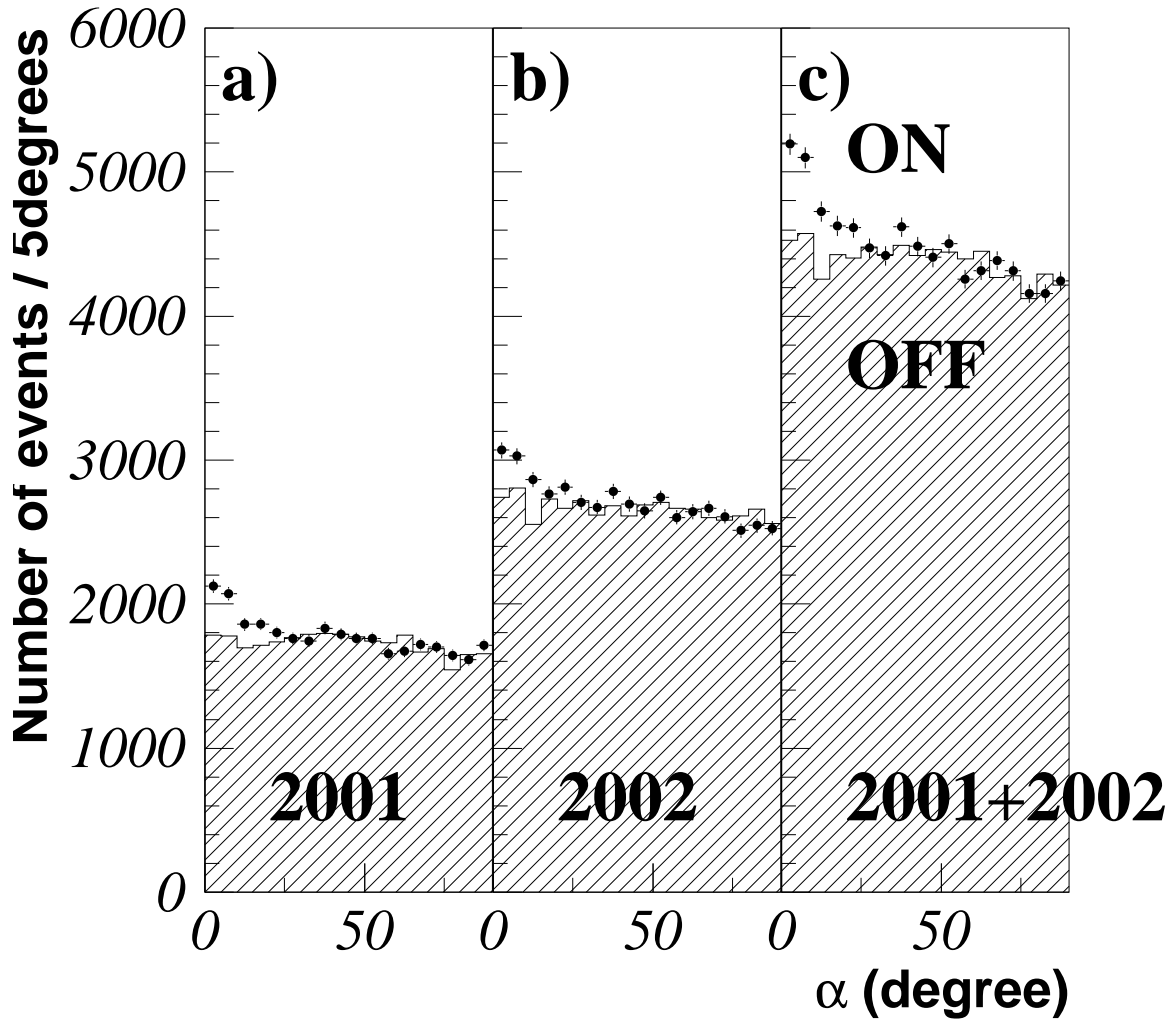


Fig. 1.— Distributions of α (image orientation angle). From left to right, the a) 2001 data, b) 2002 data, and c) combined data, are shown. The points with error bars show the ON-source data and the hatched histograms are the normalized OFF-source data.

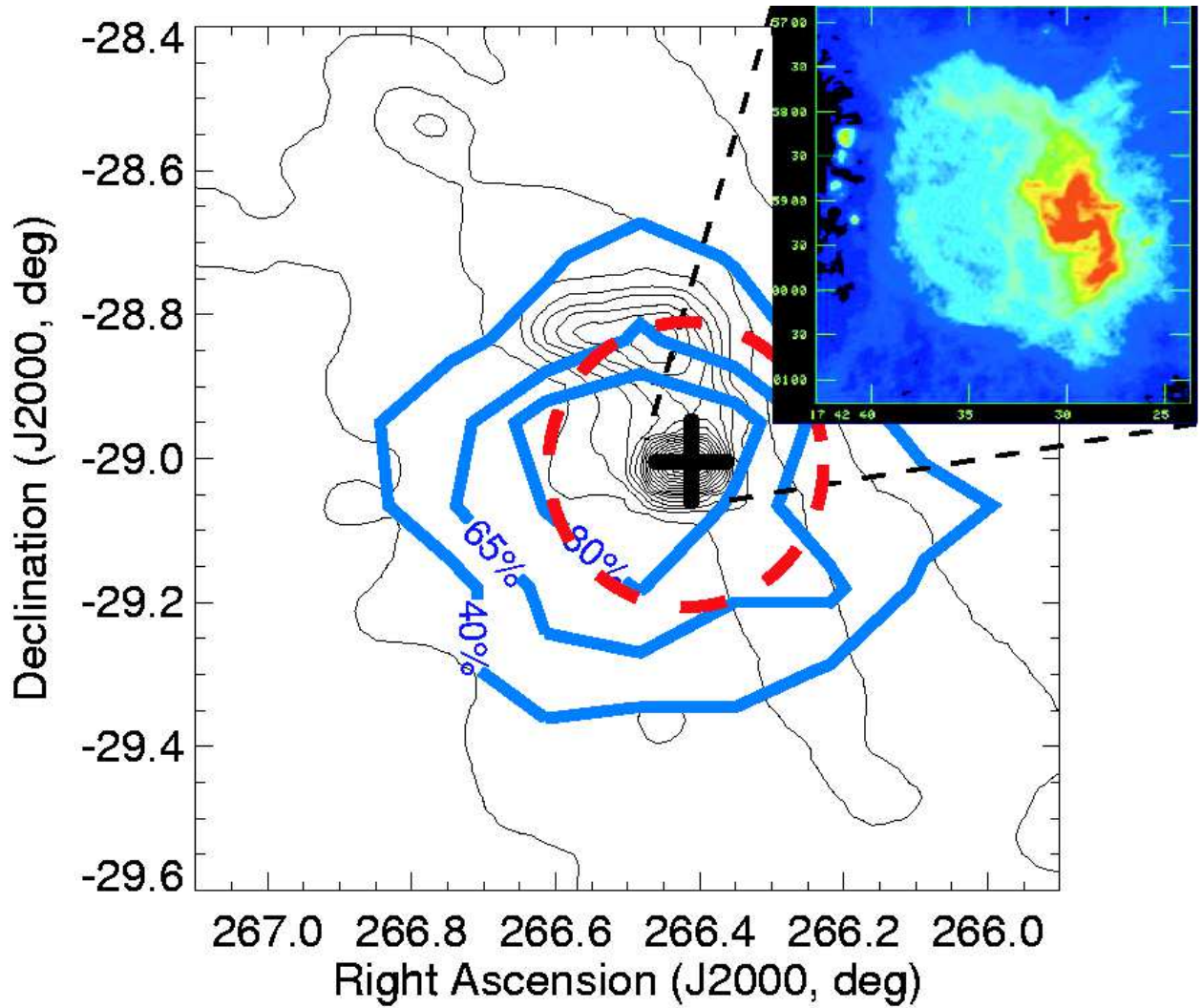


Fig. 2.— The “significance map” obtained by the CANGAROO-II telescope is shown by the blue contours. The thin contours are a 12μ IRAS image. The position of Sgr A* (the telescope tracking center) is given by the cross. The inset is a 5 GHz VLA image showing Sgr A* and Sgr A East (Yusef-Zadeh & Morris 1987). The uncertainty in the position for 3EG J1746–2851 analysed by Mayer-Hasselwander et al. (1998) is indicated by the orange dashed contour.

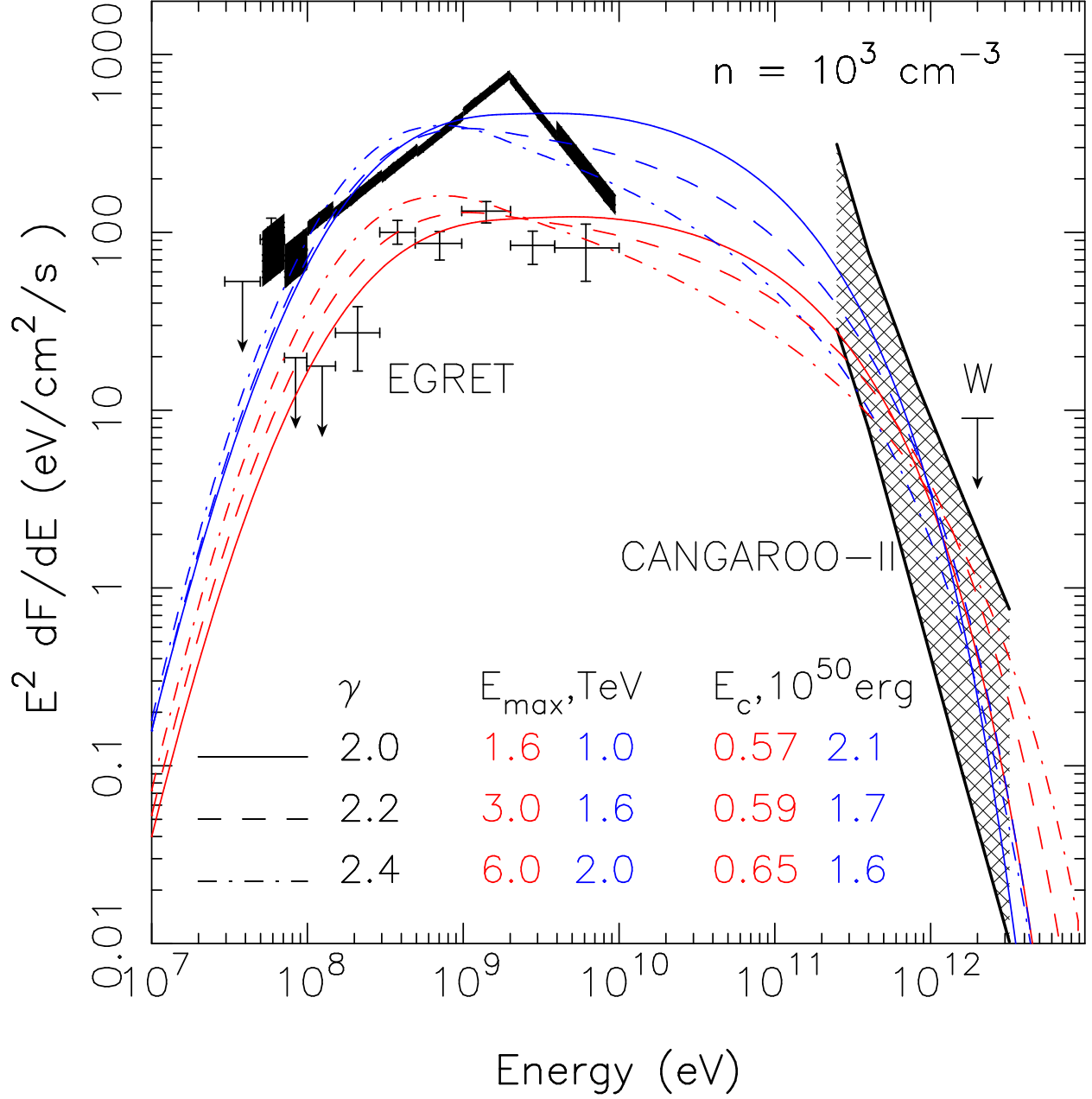


Fig. 3.— Spectral energy distribution of the GC region. The cross-hatched area is the 1σ allowed region for the TeV observations in the energy range of Table 1. Here the energy uncertainties in Table 1 were assumed to be correlated bin by bin. The arrow (W) is the Whipple 2σ upper limit at 2 TeV (Buckley et al. 1997). The two analyses of the EGRET data are shown by the black hatched region (Mayer-Hasselwander et al. 1998) and the crosses (Hartman et al. 1999). The lines are estimations for π^0 gamma-rays, the details of which are given in the body of the figure and in the text.

Table 1: Differential fluxes.

Mean energy of bin [GeV]	Flux [ph/cm ² /s/TeV]
258±64	(0.14±0.06)×10 ⁻⁸
299±66	(0.82±0.22)×10 ⁻⁹
367±80	(0.20±0.08)×10 ⁻⁹
540±102	(0.54±0.19)×10 ⁻¹⁰
962±356	(0.30±0.28)×10 ⁻¹¹
2454±653	(0.73±1.19)×10 ⁻¹³